Probing anisotropic interaction potentials of unsaturated hydrocarbons with He*(2 ^3S) metastable atom: Attractive-site preference of σ-direction in C_2H_2 and π-direction in C_2H_4

Takuya Horio, Takuro Hatamoto, Satoshi Maeda, Naoki Kishimoto, and Koichi Ohno[a)]
Department of Chemistry, Graduate School of Science, Tohoku University, Aramaki, Aoba-ku, Sendai 980-8578, Japan

(Received 14 November 2005; accepted 26 January 2006; published online 14 March 2006)

State-resolved collision energy dependence of Penning ionization cross sections of acetylene (C_2H_2) and ethylene (C_2H_4) with He*(2 ^3S) metastable atoms was observed in a wide collision energy range from 20 to 350 meV. A recently developed discharge nozzle source with a liquid N_2 circulator was employed for the measurements in the low-energy range from 20 to 80 meV. Based on classical trajectory calculations for the energy dependence of the partial ionization cross sections, anisotropic potential energy surfaces for the present systems were obtained by optimizing *ab initio* model potentials for the chemically related systems Li+C_2H_2 and C_2H_4. In the case of C_2H_2, the global minimum was found to be located around the H atom along the molecular axis with a well depth of 48 meV (ca. 1.1 kcal/mol). On the other hand, a dominant attractive well with a depth of 62 meV (ca. 1.4 kcal/mol) was found in the π_{CC} electron region of C_2H_4. These findings were discussed in connection with orbital interactions between molecular orbitals of the target molecules and atomic orbitals of the metastable atom. It is concluded that σ-type unoccupied molecular orbitals of C_2H_2 and a π_{CC}-type highest occupied molecular orbital of C_2H_4 play a significant role for the attractive-site preference of σ direction in C_2H_2 and π direction in C_2H_4, respectively. © *2006 American Institute of Physics*. [DOI: 10.1063/1.2178298]

I. INTRODUCTION

Anisotropy of interaction potential energy surfaces (PESs) for atom-molecule systems is of great importance in connection with solvation/adsorption phenomena, gaseous transport processes, and stereodynamics in collisional reactions.[1] High-resolution laser spectroscopic studies on weakly bound complexes have provided valuable information on the attractive part of the interaction potential in a specific relative orientation (global minimum).[2,3] On the other hand, scattering experiments have enabled us to investigate both the attractive and repulsive regions of PESs.[4–6] Generally it has been difficult to obtain detailed information on anisotropy of PES (e.g., the position and well depth of the global or local minimum) because of randomized orientation of target molecules in gas-phase experiments, however, anisotropy of the interaction PESs between unsaturated hydrocarbons and rare gas atoms has been elucidated recently by means of sophisticated molecular beam techniques and theoretical investigations.[7,8]

The interaction potential of excited rare gas atoms A^* with molecules M has also been studied for a long time, because of its fundamental importance in chemi-ionization processes. Especially, measurements of collision energy (E_c) dependence of the *total* Penning ionization ($A^*+M \rightarrow M_i^+ +A+e^-$) (Ref. 9) cross section σ_T have been performed extensively by detecting all ions produced, since σ_T provides information on PES between A^* and M (e.g., the well depth and the shape of repulsive wall for atomic targets).[10–16] Based on the electron exchange model proposed by Hotop and Niehaus,[17] an electron of a molecular orbital (MO) ϕ of M is transferred to the inner vacant orbital χ of A^*, and simultaneously an excited electron of A^* is ejected. This indicates that *partial* ionization cross sections σ_i for producing each ionic state of M (M_i^+) (branching ratios) depend on the mutual overlap between the corresponding MO ϕ_i and the inner vacant orbital χ of A^*. It has been found that experimental branching ratios obtained by Penning ionization electron spectroscopy[18,19] can be related to the electron density outside the repulsive surface of a target molecule M [exterior electron density (EED)].[20,21] Since the electron distribution of each MO in a target molecule is highly anisotropic, one can derive information on the anisotropy of PES from collision energy dependence of partial ionization cross sections [CEDPICS, $\sigma_i(E_c)$] even for randomly oriented target molecules, while such information cannot be obtained by measurements of σ_T. From this point of view, CEDPICS for molecular targets was first measured by utilizing an electron spectroscopic technique combined with a time-of-flight (TOF) method and a high-flux He*(2 ^3S) (excitation energy =19.82 eV) beam.[22,23] Further, collision-energy-resolved Penning ionization electron spectrum[24,25] (CERPIES) has been observed at well-defined E_c by means of supersonic molecular beams for metastable atoms and target molecules.[24,26,27] Two-dimensional (E_c and electron energy E_e) Penning ionization electron spectroscopy (2D-PIES) has

[a)]Author to whom correspondence should be addressed. Fax: +81-22-795-6580. Electronic mail: ohnok@qpcrkk.chem.tohoku.ac.jp

been developed in the last decade[28] and enabled us to observe not only CEDPICS but also CERPIES.

Theoretical investigations of interaction PES between A^* and M are also important to elucidate the anisotropic feature as well as collision dynamics. Penning ionization for simple molecular targets such as H_2 (Refs. 29 and 30) and N_2 (Refs. 31 and 32) has been investigated based on the theory established by Nakamura[33] and Miller.[34] According to this theory, both the ionization width and the interaction potentials are needed to describe collisional ionization dynamics. CEDPICS for the $N_2+He^*(2\,^3S)$ system was first simulated by classical trajectory calculations based on an *ab initio* interaction PES and ionization widths with various approximations.[31,32] Although a recent *ab initio* calculation of an interaction PES for atomic targets has succeeded in accounting for the observed E_c dependence of the ionization cross section,[35,36] it has been quite difficult to obtain reliable PES under *ab initio* treatments for molecular targets. This is caused by the difficulties in describing highly anisotropic interaction potentials for A^*-M systems embedded in an ionization continuum higher than the ionization potential (IP) of M. Ogawa and Ohno performed classical trajectory calculations for $N_2+He^*(2\,^3S)$ by utilizing a Li model PES (Ref. 37) based on the well-known similarity between metastable rare gas atoms and corresponding alkali atoms in interactions with various atomic targets.[38–41] It has been found that Li model potentials should be modified and optimized to the observed CEDPICS in order to obtain reliable interaction PES between A^* and M. Very recently, an overlap expansion method improving *ab initio* PES has been proposed for atom-molecule interaction systems on the basis of the fact that intermolecular interactions are more or less related to overlaps of MOs concerned.[42] This correction method has been designed to construct effectively anisotropic interaction PES by expanded terms utilizing overlap integrals between target MOs ϕ_i and an atomic orbital.

The 2D-PIES technique combined with classical trajectory calculations based on the overlap correction method has enabled us to investigate the anisotropy of PESs between a $He^*(2\,^3S)$ metastable atom and several molecular targets, such as N_2,[42] CO,[42] OCS,[43] CH_3CN,[44] C_2H_2,[42,43] and C_6H_6.[45] In the case of N_2 and CO, repulsive characteristics and anisotropy of the interaction PES have been elucidated in detail.[42] In the case of OCS and CH_3CN, attractive interaction has been found in the lone-pair electron regions.[43,44] The π_{CC} electron regions for C_2H_2 and C_6H_6 were also found to be attractive.[42,43,45] Furthermore, theoretical investigations on the PES for the $C_2H_2+He^*(2\,^3S)$ system suggested for the first time that a stereospecific attractive well with a depth of ca. 40 meV (~1 kcal/mol) should be expected to lie around the hydrogen atom.[42,43] However, it has not been confirmed experimentally since measurements of CEDPICS at collision energies less than 50 meV could not be performed. This is due to a reduction of electron signals caused by weak intensity of low velocity $He^*(2\,^3S)$ atom beams.

Very recently, we have developed a cooled discharge nozzle source with a liquid N_2 circulator for $He^*(2\,^3S)$ metastable atoms in order to obtain CEDPICS for molecules in the low collision energy range from 20 to 80 meV.[44] In the study of $CH_3CN+He^*(2\,^3S)$ system, a stereospecific attractive well with a depth of 38 meV around the methyl group ($-CH_3$) has been found for the first time,[44] which may be a similar situation with respect to the attractive well around hydrogen atom suggested in the $C_2H_2+He^*(2\,^3S)$ system.

In this work, CEDPICS for the $C_2H_2+He^*(2\,^3S)$ system has been measured in the collision energy range from 20 to 350 meV in order to verify the attractive well around a hydrogen atom. Although preliminary measurements of CEDPICS for this system have been reported previously,[46] a full account on the observed CEDPICS is given in this article. Furthermore, we have tried to obtain the interaction PES between C_2H_2 and $He^*(2\,^3S)$ by utilizing the new experimental data of CEDPICS and the above theoretical method (the overlap correction of an *ab initio* Li model potential). The $C_2H_4+He^*(2\,^3S)$ system has also been investigated by the same method. In addition, the optimized PESs for both systems have been discussed in terms of orbital interactions between MOs of the hydrocarbon molecules and atomic orbitals of the $He^*(2\,^3S)$ metastable atom.

II. EXPERIMENT

A detailed description about the present apparatus has been reported previously.[44] Metastable atom beams of $He^*(2\,^1S, 2\,^3S)$ were produced by a nozzle discharge source with a tantalum hollow cathode and a conical skimmer (orifice diameter=0.7 mm) for an anode. A machined piece of boron nitride (BN) nozzle cap (orifice diameter=0.8 mm) was attached onto a Pyrex glass pipe for introducing helium gas (purity > 99.999 95%). This nozzle cap can be cooled by a liquid N_2 circulator for experiments in lower collision energies ranging from 20 to 80 meV. The metastable beams were pulsed by a mechanical chopper (100 mm diam and 0.2 mm thick) with a slit width of 2 mm rotating between 240 and 320 Hz for TOF measurements. The $He^*(2\,^1S)$ metastable atoms were optically removed by a water-cooled He discharge (quenching) lamp. Typical values of the average velocity for the $He^*(2\,^3S)$ beams were 1300 m/s at the discharge power of 6 W with the liquid N_2 circulator, and 2300 m/s at the discharge power of 13 W without the liquid N_2 cooling. Sample gases of C_2H_2 and C_2H_4 were introduced into an ionization region from an effusive beam source (nozzle diameter=1.5 mm). The base pressure in the reaction chamber was 3×10^{-8} Torr, and the measurements were carried out under the pressure of 2.2×10^{-6} Torr with both beams on.

The kinetic energy of ejected electrons was measured by means of an electrostatic retarding-field-type analyzer equipped with an electron flight tube. This analyzer employs the "magnetic bottle effect"[47–49] utilizing an inhomogeneous magnetic field with a permanent magnet and a guiding solenoid for high efficient measurements.[50] Magnetic fields at the ionization region and in the flight tube are ca. 80 and 1.4 mT, respectively. The ejected electrons were decelerated by the retarding electrodes and then accelerated to the former speed.

The electrons that passed through the retarding fields were detected by a dual microchannel plate (MCP) placed at the end of the flight tube.

For collision-energy-resolved measurements, electron signals $I_e(E_e,t)$ as functions of electron kinetic energy (E_e) and TOF of the metastable $He^*(2\,^3S)$ atoms between the collision center and the chopper disk (flight length=735 mm) were stored in a two-parameter multichannel scaler equipped with a retarding voltage generator (Laboratory Equipment Corporation, VSCANMCS NT-2400M) at a typical time resolution of 2 μs, a step of electron-energy scan of 40 meV, and a dwell time of 100 ms. The $I_e(E_e,t)$ can be converted to $I_e(E_e,v_{He^*})$ as functions of E_e and the velocity of metastable He^* atoms (v_{He^*}). The two-dimensional Penning ionization cross section $\sigma(E_e,v_r)$ with normalization by the velocity distribution of He^* atoms I_{He^*} (v_{He^*}) was obtained by the following equations:

$$\sigma(E_e,v_r) = c\frac{I_e(E_e,v_{He^*})}{I_{He^*}(v_{He^*})}\frac{v_{He^*}}{v_r}, \tag{1}$$

$$v_r = \sqrt{v_{He^*}^2 + v_M^2}, \tag{2}$$

where c is a constant, v_r is the relative velocity between the $He^*(2\,^3S)$ atom and the target molecule, and v_M is the velocity of the target molecule. Under an effusive beam condition, v_M was obtained by averaging over the velocity of the target molecule,

$$v_M = \sqrt{\frac{3k_BT}{m_M}}, \tag{3}$$

where k_B is the Boltzmann constant, T is the temperature of the effusive nozzle (298 K), and m_M is the mass of the target molecule. The velocity distribution $I_{He^*}(v_{He^*})$ was determined by monitoring secondary electrons emitted from an inserted stainless steel needle. It should be noted that TOF of the ejected electrons to reach the electron detector (MCP) from the ionization region (<0.5 μs) can be negligible in comparison with that of the metastable $He^*(2\,^3S)$ atoms to reach the collision center from the chopper disk (200–800 μs). Finally, $\sigma(E_e,v_r)$ is converted to the final form $\sigma(E_e,E_c)$,

$$E_C = \frac{1}{2}\mu v_r^2, \tag{4}$$

where μ is the reduced mass of the colliding system.

III. CALCULATIONS

A. Interaction potential energy surface

For anisotropic molecular targets, it has been difficult to evaluate interaction potentials in good accuracy under *ab initio* treatments, since the electronic state with a large excitation energy of a He atom is embedded in continuum states much higher than the ionization threshold of the target molecules. In this point of view, we first calculated an approximate interaction PES V_0 using $Li(2\,^2S)$ in place of $He^*(2\,^3S)$ on the basis of the well-known resemblance between $He^*(2\,^3S)$ and $Li(2\,^2S)$ (Refs. 38–41) (V_0: Li model potential). *Ab initio* MO calculations of V_0 for both systems of C_2H_2+Li and C_2H_4+Li were performed using a GAUSSIAN quantum chemistry program[51] at the coupled cluster level of theory including single, double, and optional triple excitation CCSD(T) with 6-311++G^{**} basis set. The Li model potential V_0 between the target molecule M and a Li atom can be obtained by the following manner:

$$V_0 = E_{M\mathrm{Li}} - (E_M + E_{\mathrm{Li}}). \tag{5}$$

Here, $E_{M\mathrm{Li}}$, E_M, and E_{Li} are the total energies of a supermolecule MLi, an isolated molecule M, and an isolated Li atom, respectively. The basis-set super position error (BSSE) was corrected by the full counterpoise method.[52] The experimental equilibrium geometry was used for each molecule, and then the interaction PES V_0 can be expressed as functions of R and θ for the C_2H_2+Li system, where R is the distance between a Li atom and the center of mass of C_2H_2, and θ is the polar angle from the molecular axis. In the case of the C_2H_4+Li system, V_0 was obtained as functions of R, θ, and ϕ, where R is the distance between a Li atom and the center of mass of C_2H_4, θ denotes the polar angle from the C_2 symmetry axis parallel to the C=C double bond, and ϕ is the azimuthal angle.

Although $Li(2\,^2S)$ has the same valence electronic configuration as $He^*(2\,^3S)$ with a 2s electron that predominantly contributes to intermolecular interactions, it is natural that orbital interactions between $Li(2\,^2S)$ and target molecules should differ to some extent from those of $He^*(2\,^3S)$. Thus, in order to obtain anisotropic interaction potential V^* between target molecules and a $He^*(2\,^3S)$ atom more quantitatively, the Li model potential V_0 should be optimized to better reproduce experimental observations of CEDPICS. In the present calculations, the overlap expansion (OE) method[42] was used for improving the *ab initio* model potentials. In the OE method, the Li model PES $V_0(R,\theta,\phi)$ can be modified with the following equations to obtain the $V^*(R,\theta,\phi)$ for the present systems (ϕ is not a parameter in the C_2H_2+Li system):

$$V^*(R,\theta,\phi) = V_0(R,\theta,\phi) - \sum_i C_i|\langle\phi_i|\chi\rangle|^2, \tag{6}$$

$$\chi = \sqrt{\zeta^3/\pi}\exp[-\zeta r]. \tag{7}$$

Here, χ is a Slater-type s orbital function with an exponent ζ, which is located at the position of the He^*/Li atom. r is the distance from the center of χ. This correction method has been developed to describe effectively anisotropic interaction PESs by expanded terms using overlap integrals between target MOs ϕ_i concerned and an atomic orbital χ. As reported in the previous studies for several molecular targets,[42–45] the optimized values of ζ in Eq. (7) have been found to be very close to the exponent of the 2s orbital of He^* atom, which is 0.575 bohr^{-1} according to Slater's rule. This allows us to fix the ζ parameter in Eq. (7) to the above value. The expansion coefficients C_i are parameters to be optimized in the present potential corrections. In trial calculations, we found that the following MOs ϕ_i should be employed in the correction term: $2\sigma_u$, $3\sigma_g$, $1\pi_u$, $4\sigma_g$, $3\sigma_u$, and $1\pi_g$ orbitals for C_2H_2, and $1b_{3u}$, $3a_g$, $1b_{2g}$, $1b_{2u}$, $4a_g$, $3b_{1u}$,

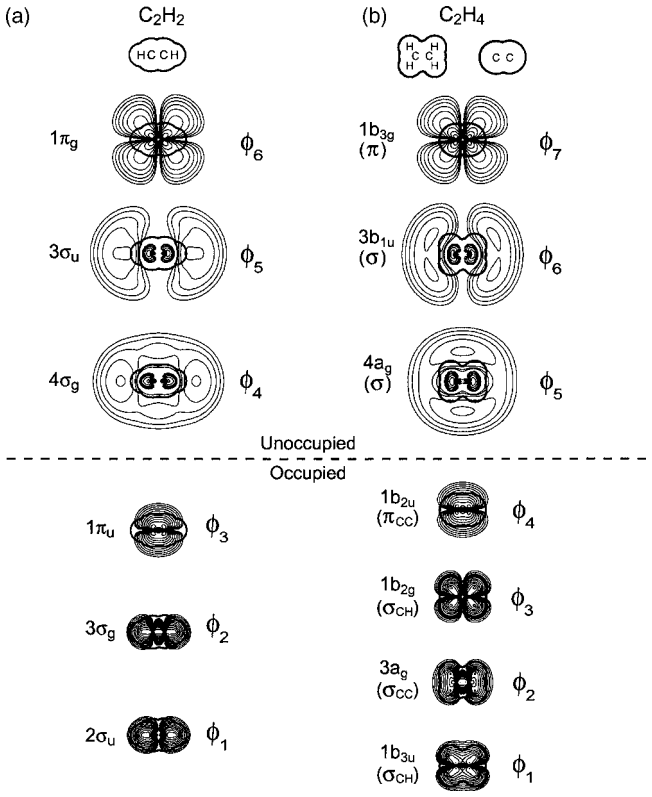

FIG. 1. Contour maps of electron density distribution of MOs of (a) C_2H_2 and (b) C_2H_4 used for optimizations of potential energy surface (see text in Sec. III). In the case of C_2H_4, the cutting plane for the electron density contour curves for the σ-type MOs is the molecular plane, while for the π orbitals ($1b_{2u}$ and $1b_{3g}$), the electron density contour curves are taken in the σ_v vertical plane that includes the C=C double bond.

and $1b_{3g}$ orbitals for C_2H_4. The electron density contour maps of the respective MOs with the numbering of $\phi_i(C_i)$ for C_2H_2 and C_2H_4 are shown in Figs. 1(a) and 1(b), respectively. In the case of C_2H_4, the cutting plane for the electron density contour curves for the σ-type MOs is the molecular plane, while for π orbitals ($1b_{2u}$ and $1b_{3g}$), the electron density contour curves are taken in the σ_v vertical plane that includes the C=C double bond. These MOs were obtained by *ab initio* self-consistent field (SCF) calculations for respective molecules with 6-311++G** basis set. The molecular shapes estimated approximately from van der Waals radii of component atoms are also shown schematically with thick solid lines in Fig. 1.

B. Ionization widths

The ionization width $\Gamma^{(i)}$ for the ith ionic state is given by

$$\Gamma^{(i)} = 2\pi\rho^{(i)}|\langle\Phi_0|H_{\mathrm{el}}|\Phi^{(i)}\rangle|^2. \tag{8}$$

Here $\rho^{(i)}$ is the density of final states. H_{el} is the electronic Hamiltonian, and Φ_0 and $\Phi^{(i)}$ are electronic wave functions for the initial and ith final states, respectively. Slater determinant wave functions composed of one-electron orbitals for both initial and final states give the following formula for the integral in Eq. (8):

$$\langle\Phi_0|H_{\mathrm{el}}|\Phi^{(i)}\rangle \approx \langle\chi_{2s}(1)\phi_i(2)|r_{12}^{-1}|\chi_{1s}(1)\phi_\varepsilon(2)\rangle - \langle\chi_{2s}(1)\phi_i(2)|r_{12}^{-1}|\chi_{1s}(2)\phi_\varepsilon(1)\rangle, \tag{9}$$

where χ_{2s} and ϕ_i are the $2s$ orbital of He^* and the ith orbital of the target molecule in the initial states, respectively, and χ_{1s} and ϕ_ε are the He $1s$ orbital and the outgoing ejected electron orbital in the final state, respectively. The first term in Eq. (9) vanishes for $He^*(2\,^3S)$ due to the spin inversion. By replacing r_{12} with a suitable average value, the second term in Eq. (9) can be approximated as a product of two overlap integrals with a constant factor C,[53]

$$C\langle\phi_i|\chi_{1s}\rangle\langle\chi_{2s}|\phi_\varepsilon\rangle. \tag{10}$$

Such an approximation has been widely used in semiempirical molecular orbital theories[54] as well as in semiempirical treatments for electron transport phenomena. Since the $2s$ and outgoing electron orbitals are very diffuse, anisotropy of the ionization width is governed by the compact He $1s$ orbital and the ionized molecular orbital. Thus, the following formula can be used for the estimation of the ionization width into ith ionic state:

$$\Gamma^{(i)} = K^{(i)}|\langle\phi_i|\chi_{1s}\rangle|^2, \tag{11}$$

where $K^{(i)}$ is a parameter to be determined in order to reproduce observed relative branching ratio and collision energy dependence for respective ionic states. Using this treatment, one can also avoid theoretical and computational difficulties associated with direct calculations of the matrix elements including highly excited states for too many geometrical configurations. The orbital functions for the target molecules and He atom in Eq. (11) were obtained by SCF calculations with 6-311++G** basis set.

C. Classical trajectory calculations for CEDPICS and potential optimizations

In order to obtain CEDPICS, classical trajectory calculations on interaction PESs were made by the following way.[37,43] The relative motion of the colliding systems was determined by solving the equation of motion. At each trajectory step of an interval dt, transition probabilities $P^{(i)}\times(t)dt$ into each ionic state i can be expressed by

$$P^{(i)}(t)dt = S(t)\frac{\Gamma^{(i)}}{\hbar}dt, \tag{12}$$

$$S(t) = 1 - \sum_i P_{\mathrm{int}}^{(i)}(t), \tag{13}$$

where the survival fraction $S(t)$ is the probability of $He^*(2\,^3S)$ surviving in the excited state at a certain time t and then $P_{\mathrm{int}}^{(i)}$ represents the integrated partial ionization probability before time t. Calculations of 10 000 trajectories were performed for a given collision energy E_c, where initial conditions for the impact parameter b(0–9 Å), the molecular orientation, and the direction of the rotational angular momentum vector of the target molecules were randomly generated. The initial energy of the molecular rotation was obtained by a random generation technique so that the distribution obeys Boltzmann distribution at room tempera-

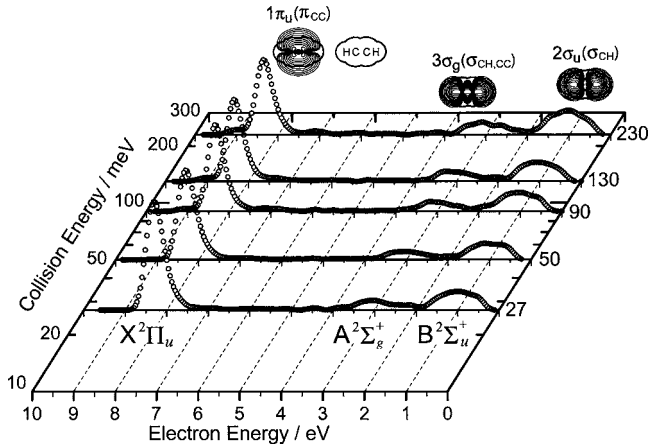

FIG. 2. Observed collision-energy-resolved Penning ionization electron spectra (CERPIESs) of C_2H_2 at collision energies of ca. 27, 50, 90, 130, and 230 meV. The calculated electron density contour maps of SCF-MOs corresponding respective ionic states are also shown.

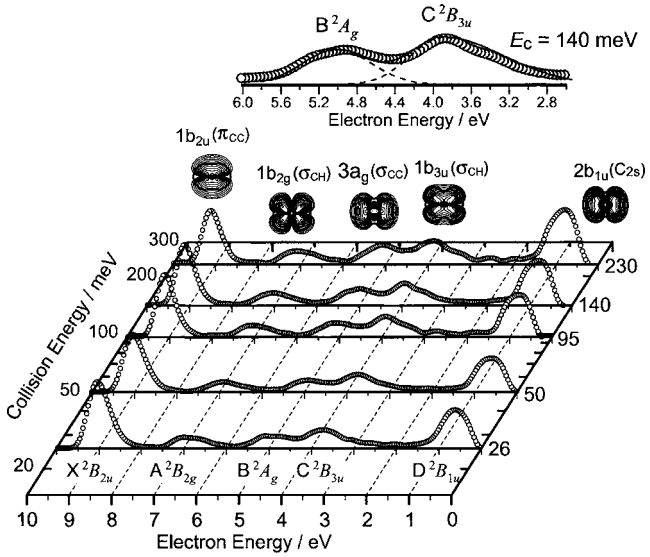

FIG. 3. Observed collision-energy-resolved Penning ionization electron spectra (CERPIESs) of C_2H_4 at collision energies of ca. 26, 50, 95, 140, and 230 meV. The calculated electron density contour maps of SCF-MOs corresponding respective ionic states are also shown. An inset shows an expanded view of CERPIES at E_c=140 meV in the electron-energy range from 2.6 to 6.0 eV. Deconvoluted bands for $B\ ^2A_g$ and $C\ ^2B_{3u}$ ionic states with asymmetric Gaussian functions, and a fitted spectrum are shown with dashed lines, and a solid line, respectively.

ture to match the experimental condition. Because of the difficulty in estimating intramolecular motions during the collisional processes, the molecular structure of the target molecules was fixed at the experimental geometry. Structural deformation of the target molecules during the collisional processes will be discussed in Sec. IV C.

Finally, the partial ionization cross section $\sigma^{(i)}$ was obtained from the partial ionization probability $P^{(i)}$ of a trajectory,

$$\sigma^{(i)} = \int_0^\infty 2\pi b P^{(i)} db. \tag{14}$$

The parameters of C_i and $K^{(i)}$ in Eqs. (6) and (11) were optimized by a nonlinear least square fitting method in order to reproduce the slopes and branching ratios in the observed CEDPICS.

IV. RESULTS AND DISCUSSION

A. Ionic states of C_2H_2 and C_2H_4

Figure 2 shows the collision-energy-resolved Penning ionization electron spectra of C_2H_2 at collision energies of ca. 27, 50, 90, 130, and 230 meV. Judging from the known ultraviolet photoelectron spectrum (UPS) of C_2H_2,[55] it is clear that produced ionic states of $C_2H_2^+$ denoted by $X\ ^2\Pi_u$, $A\ ^2\Sigma_g^+$, and $B\ ^2\Sigma_u^+$ correspond to ionization from $1\pi_u(\pi_{CC})$, $3\sigma_g(\sigma_{CH}(\sigma_{CC}))$, and $2\sigma_u(\sigma_{CH})$ MOs, respectively. Figure 3 shows the collision-energy-resolved Penning ionization electron spectra of C_2H_4 at collision energies of ca. 26, 50, 95, 140, and 230 meV. Based on the observed UPS of C_2H_4,[55] ionic states of $C_2H_4^+$ denoted by $X\ ^2B_{2u}$, $A\ ^2B_{2g}$, $B\ ^2A_g$, $C\ ^2B_{3u}$, and $D\ ^2B_{1u}$ can be ascribed to ionization from $1b_{2u}(\pi_{CC})$, $1b_{2g}(\sigma_{CH})$, $3a_g(\sigma_{CC})$, $1b_{3u}(\sigma_{CH})$, and $2b_{1u}$(C2s) MOs, respectively.

It should be noted that the MOs for both C_2H_2 and C_2H_4 are roughly classified into two classes of π and σ orbitals according to their symmetries. The calculated electron density contour maps of SCF-MOs corresponding to ionic states of C_2H_2 and C_2H_4 are also shown in Figs. 2 and 3, respectively. In the case of C_2H_2, $1\pi_u(\pi_{CC})$ MO has a large extent of the electron distribution perpendicular to the molecular axis (HCCH), while $3\sigma_g(\sigma_{CH(CC)})$ and $2\sigma_u(\sigma_{CH})$ MOs have a large extent of the electron distribution collinear to the molecular axis. In the case of C_2H_4, π electrons [$1b_{2u}(\pi_{CC})$ MO] mainly distribute out of the molecular plane. The σ electrons [$1b_{2g}(\sigma_{CH})$, $3a_g(\sigma_{CC})$, $1b_{3u}(\sigma_{CH})$, and $2b_{1u}$(C2s) MOs] largely distribute in the in-plane directions. Since the ionization from MOs having a C_{2s} character cannot be described by the electron exchange model in the Penning ionization,[25,56] the $D\ ^2B_{1u}$ ionic state of $C_2H_4^+$ has not been included in the present trajectory calculations.

B. Characteristic features of CEDPICS

Figures 4 and 5 show the observed log σ (cross section)-log E_c (collision energy) plots of CEDPICS (open circles) for C_2H_2 and C_2H_4, respectively. The calculated electron density contour maps of SCF-MOs corresponding to respective ionic states are also shown in Figs. 4 and 5. The observed slope parameters m for the log σ vs log E_c plots are summarized in Tables I and II. Table I lists the slope parameters m for C_2H_2 in collision energy regions of 20–50, 50–100, and 100–320 meV. Table II also lists the parameters m for C_2H_4 in collision energy regions of 20–50, 50–100, and 100–310 meV. The values of m in Tables I and II were obtained by the least-squares method. It should be noted that the present measurements on CEDPICS in higher collision energies (100–300 meV for C_2H_2 and 50–350 meV for C_2H_4) gave much better qualities of the observed data than the previous results.[25,42,57]

Figures 4 and 5 also compare the observed CEDPICS with the calculated one obtained by classical trajectory calculations utilizing the optimized PESs V^*. The vertical axis in Figs. 4 and 5 represents the calculated ionization cross

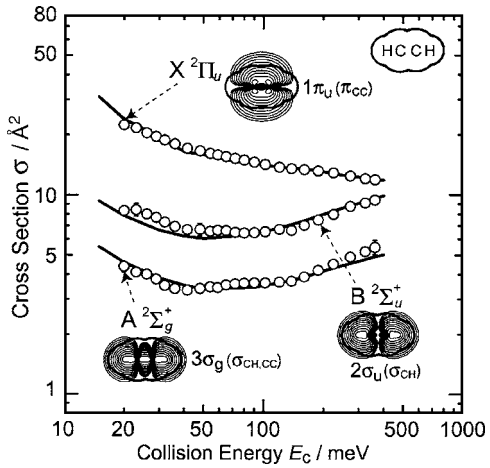

FIG. 4. Observed log σ (cross section)-log E_c (collision energy) plots of CEDPICS for C_2H_2 are shown with circles. The calculated CEDPICSs obtained by the classical trajectory calculations utilizing the optimized potential energy surface V^* are also drawn with solid lines.

section that is given from the optimization procedure, as mentioned in Sec. III C. In the case of C_2H_4, the partial ionization cross sections for the ionic states of $B\,^2A_g$ and $C\,^2B_{3u}$ were estimated by decomposition of the observed bands into asymmetric Gaussian functions at E_c=140 meV (broken lines in an inset in Fig. 3), at which the most reliable electron spectra can be obtained in our experimental setup because of high He^* beam intensity.

As can be seen from the comparison of the observed CEDPICS with the calculated one in Figs. 4 and 5, the present trajectory calculations using the optimized PESs of V^* well account for the observed features of CEDPICS in the studied collision energy range. The values of the calculated total ionization cross sections [ca. 30 Å^2 at E_c=33 meV for both molecules ($D\,^2B_{1u}$ state was not included in C_2H_4)] were also found to be roughly comparable to those estimated by pulse radiolysis methods for $He^*(2\,^3S)$ metastable atoms with the present molecules (ca. 40 Å^2 at the same E_c).[58]

General features in CEDPICS of C_2H_2 and C_2H_4 are similar to each other (see Figs. 4 and 5) and can be summarized as follows.

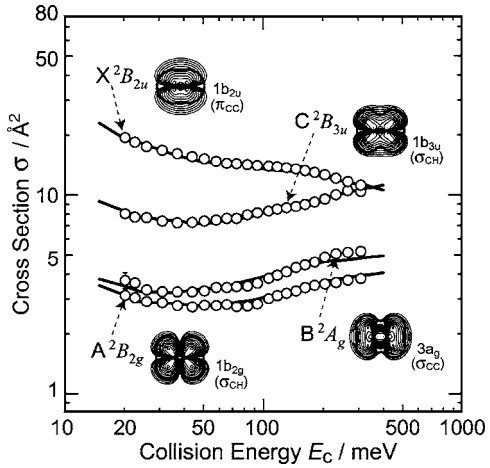

FIG. 5. Observed log σ (cross section)-log E_c (collision energy) plots of CEDPICS for C_2H_4 are shown with circles. The calculated CEDPICSs obtained by the classical trajectory calculations utilizing the optimized potential energy surface V^* are also drawn with solid lines.

TABLE I. Slope parameters m of CEDPICS for the C_2H_2+$He^*(2\,^3S)$ system in the collision energy range from 20 to 320 meV.

Ionic state	Orbital	Character	Collision energy range (meV)	m
$X\,^2\Pi_u$	$1\pi_u$	π_{CC}	20–50	−0.36±0.02
			50–100	−0.20±0.01
			100–200	−0.12±0.01
			200–320	−0.18±0.01
			100–320	−0.16±0.02
$A\,^2\Sigma_g^+$	$3\sigma_g$	σ_{CH}, σ_{CC}	20–50	−0.33±0.05
			50–100	0.11±0.02
			100–320	0.33±0.03
$B\,^2\Sigma_u^+$	$2\sigma_u$	σ_{CH}	20–50	−0.32±0.03
			50–100	−0.05±0.02
			100–320	0.30±0.03

(1) CEDPICS for ionization from π orbitals ($1\pi_u$ for C_2H_2 and $1b_{2u}$ for C_2H_4) has been found to decrease as collision energy E_c increases (negative CEDPICS) in the studied collision energy range (see also the slope parameter m in Table I and II).

(2) CEDPICS for ionization from σ orbitals ($3\sigma_g$ and $2\sigma_u$ for C_2H_2 and $1b_{2g}$, $3a_g$, and $1b_{3u}$ for C_2H_4) shows an increasing trend with the increase of E_c in the collision energy region higher than ca. 100 meV (positive CEDPICS), while negative CEDPICS has been found in the lower collision energies between 20 and 50 meV (see also the slope parameter m in Tables I and II).

It is well known that negative E_c dependence of ionization cross section in low collision energies indicates attractive interaction between a target molecule and $He^*(2\,^3S)$. Based on the previous study for isotropic targets,[59] close collisions lead to ionization that surmounts the rotational barrier in the

TABLE II. Slope parameters m of CEDPICS for the C_2H_4+$He^*(2\,^3S)$ system in the collision energy range from 20 to 310 meV

Ionic state	Orbital	Character	Collision energy range (meV)	m
$X\,^2B_{2u}$	$1b_{2u}$	π_{CC}	20–50	−0.28±0.02
			50–100	−0.12±0.02
			100–200	−0.14±0.01
			200–310	−0.29±0.01
			100–310	−0.21±0.01
$A\,^2B_{2g}$	$1b_{2g}$	σ_{CH}	20–50	−0.17±0.02
			50–100	0.01±0.03
			100–310	0.22±0.03
$B\,^2A_g$	$3a_g$	σ_{CC}	20–50	−0.18±0.05
			50–100	0.12±0.02
			100–310	0.32±0.02
$C\,^2B_{3u}$	$1b_{3u}$	σ_{CH}	20–50	−0.13±0.02
			50–100	0.15±0.03
			100–310	0.24±0.01

effective potential formed by a long-range attractive potential $V^*(R)$ and the centrifugal barrier $E_c(b^2/R^2)$ (b is the impact parameter). The collisions are characterized by impact parameters smaller than the critical impact parameter b_c, for which the colliding system reaches the top of the effective potential at a given collision energy E_c. In this case, if the function form of the long-range attractive part of $V^*(R)$ is the type of

$$V^*(R) \propto -R^{-s}, \tag{15}$$

the critical impact parameter b_c is proportional to $E_c^{-1/s}$. Thus, as long as the ionization probability for collisions with the impact parameter b smaller than b_c is constant, collision energy dependence of the ionization cross section $\sigma(E_c)$ can be expressed by[10,12,23,59]

$$\sigma(E_c) \propto E_c^{-2/s}. \tag{16}$$

This formula can be given in the condition that collision energy is less than the depth of attractive potential well D ($E_c < D$). In the condition of $E_c > D$, the repulsive part of $V^*(R)$ is decisively important to characterize $\sigma(E_c)$. In addition, trajectories having small impact parameters mainly contribute collisional ionization. When simple analytical forms for $V^*(R)$ and the transition probability $W(R)$ are employed as

$$V^*(R) = B \exp(-dR) \tag{17}$$

and

$$W(R) = C \exp(-gR), \tag{18}$$

$\sigma(E_c)$ can be expressed by[10,12,23]

$$\sigma(E_c) \propto E_c^{(g/d)-(1/2)}. \tag{19}$$

The parameter d is related to the effective steepness of the repulsive potential wall in $V^*(R)$, and g is the effective decay parameter of $W(R)$. As discussed previously,[23] the parameter g can be evaluated from the asymptotic decay of the target wave function, which is directly connected with the first ionization potential of the target molecule M[IP(M)],[60,61]

$$g = 2[2\mathrm{IP}(M)]^{1/2}. \tag{20}$$

As shown in Eq. (20) the parameter g is a constant for a given target molecule, thus $\sigma(E_c)$ can be related to the repulsive part of $V^*(R)$. In the higher collision energy limit, the parameter d in $V^*(R)$ tends to be very large because of a hard-sphere collision regime, and then, the ratio of g/d in Eq. (19) becomes negligibly small. In this case, $\sigma(E_c)$ shows negative collision energy dependence due to a factor of $-1/2$ in Eq. (19), which indicates that ionization cross section is governed by effective interaction time in impact collisions.

In Secs. IV C and IV D, we will discuss on the observed findings in CEDPICS by taking account of the above considerations and the optimized anisotropic PESs for the present systems.

C. Interaction potential in the π electron region

Figures 6 and 7 shows the contour maps of the optimized PESs of V^* for C_2H_2+He*($2\,^3S$) and C_2H_4+He*($2\,^3S$), respectively. In the case of C_2H_4, Fig. 7 shows the $V^*(R,\theta,\phi)$ contour maps taken in (a) the σ_v vertical plane that includes the C=C double bond of C_2H_4 (ϕ=0°) and (b) the molecular plane of C_2H_4 (ϕ=90°). The energy spacing of the contour lines of V^* for negative values in 10 meV for the energy

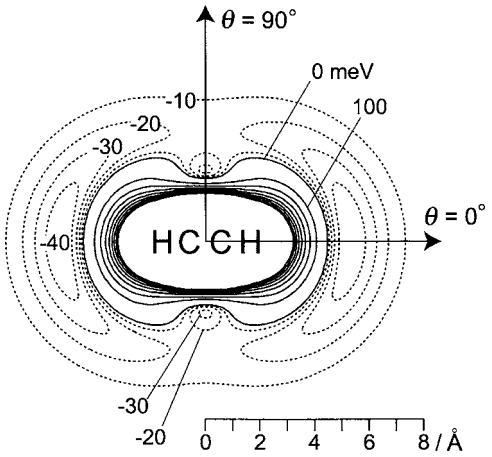

FIG. 6. Contour map of the optimized potential energy surface $V^*(R,\theta)$ for the C_2H_2+He*($2\,^3S$) system. The positive and negative values of the potential energy are shown with solid lines and dotted lines, respectively. The energy spacing of the contour lines for the negative values is 10 meV for the energy range from −40 to −10 meV. In the case of the positive values, the energy spacing is 100 meV for the energy range from 0 to 800 meV.

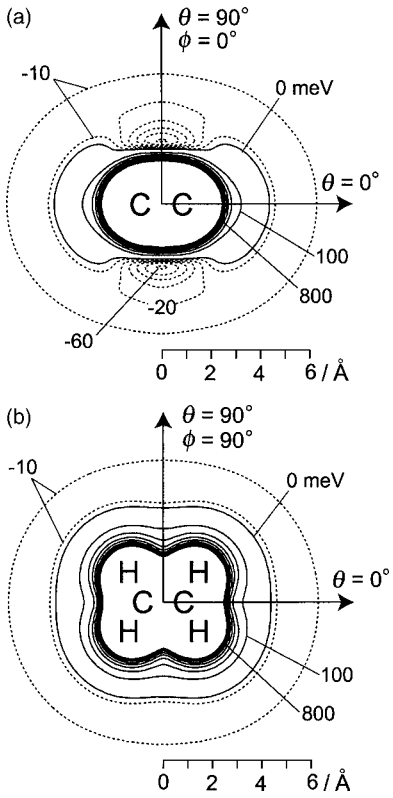

FIG. 7. Contour maps of the optimized potential energy surface $V^*(R,\theta,\phi)$ for the C_2H_4+He*($2\,^3S$) system taken in (a) the σ_v vertical plane that includes the C=C double bond of C_2H_4 (ϕ=0°) and (b) the molecular plane of C_2H_4 (ϕ=90°). The positive and negative values of the potential energy are shown with solid lines and dotted lines, respectively. The energy spacing of the contour lines for the negative values is 10 meV for the energy range from −60 to −10 meV. In the case of the positive values, the energy spacing is 100 meV for the energy range from 0 to 800 meV.

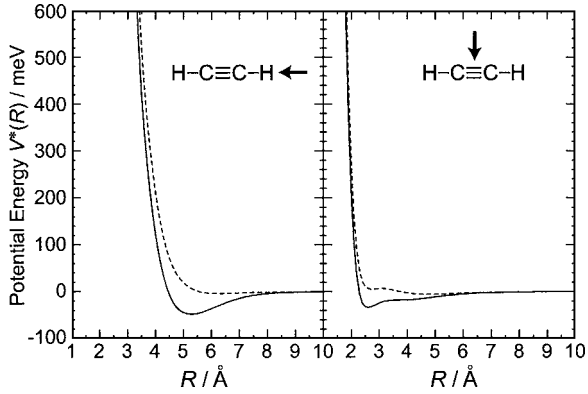

FIG. 8. Optimized interaction potential energy curves (solid lines) of $V^*(R)$ as a function of distance R between $He^*(Li)$ and the center of mass of C_2H_2 in (a) the collinear direction ($\theta=0°$) and (b) the perpendicular direction to the molecular axis ($\theta=90°$). The Li model potential curves $V_0(R)$ are also shown with broken lines.

ranges from −40 to −10 meV in Fig. 6 and from −60 to −10 meV in Fig. 7. In the case of positive values, the energy spacing is 100 meV for the energy range from 0 to 800 meV. In Fig. 8, the optimized interaction potential energy curves $V^*(R)$ for $C_2H_2+He^*(2\,^3S)$ in (a) the collinear direction ($\theta=0°$) and (b) the perpendicular direction to the molecular axis ($\theta=90°$) are shown with solid lines. The Li model potential curves $V_0(R)$ are also shown with broken lines in Fig. 8. Figure 9(a) shows $V^*(R)$ (solid lines) and $V_0(R)$ (broken lines) for $C_2H_4+He^*(2\,^3S)$ in an out-of-plane configuration ($\theta=90°$ and $\phi=0°$). Figures 9(b) and 9(c) also indicate $V^*(R)$ (solid lines+filled symbols) and $V_0(R)$ (broken lines+open symbols) for $C_2H_4+He^*(2\,^3S)$ in several in-plane configurations ($\phi=90°$) (circles: $\theta=0°$, triangles: $\theta=30°$, diamonds: $\theta=60°$, and squares: $\theta=90°$). Tables III and IV summarize the attractive well depths D_e and its geometrical positions R_e, θ_e, and ϕ_e in the optimized PESs V^* for $C_2H_2+He^*(2\,^3S)$ and $C_2H_4+He^*(2\,^3S)$, respectively.

Since Penning ionization processes crucially depend on local characteristics of electron distributions of target MOs, it is obvious that the negative CEDPICS for the X ionic states in Figs. 4 and 5 can be related to attractive interaction around the π_{CC} regions for the C_2H_2 and C_2H_4 molecules. The attractive interaction around the π_{CC} regions for unsaturated hydrocarbons was also reported in the previous experimental studies in a higher E_c range. [25,57] As can be seen in the optimized PESs and potential energy curves [see Figs. 6, 7, 8(b), and 9(a)], an attractive potential well is clearly found in the π_{CC} region for C_2H_2 and C_2H_4. In the case of C_2H_2, the well depth $D_e(\pi)$ and its geometrical positions $R_e(\pi)$ and $\theta_e(\pi)$ in the π_{CC} region were found to be 34 meV (ca. 0.8 kcal/mol), 2.6 Å, and 90.0°, respectively. In the case of C_2H_4, $D_e(\pi)$, $R_e(\pi)$, $\theta_e(\pi)$, and $\phi_e(\pi)$ were found to be 62 meV (ca. 1.4 kcal/mol), 2.6 Å, 90.0°, and 0.0°, respectively. The larger negative value of the slope parameter m in the lower E_c range (20–50 meV) for C_2H_2 ($m=-0.36$) than that for C_2H_4 ($m=-0.28$) is likely to be due to the ring-like attractive potential surrounding the C≡C triple bond of C_2H_2.

In connection with the interactions of He^* with the unsaturated hydrocarbons, charge-transfer complexes for the chemically related systems of $Li+C_2H_2$ and C_2H_4 have been observed in electron spin resonance (ESR) measurements using argon matrix isolation.[62,63] In these interacting systems, the Li atom which is excited to a ^2P state interacts strongly

TABLE III. Optimized parameters of the coefficients C_i in Eq. (6) for potential fitting and $K^{(i)}$ in Eq. (11) for ionization widths (see text) for the system of $C_2H_2+He^*(2\,^3S)$. The uncertainties of the coefficients C_i from the experimental errors of the observed slope parameters m are given in parentheses. The obtained potential well depths of $D_e(\pi)$ around the π_{CC} region and $D_e(\sigma)$ around the σ_{CH} region, and their geometrical positions of $R_e(\pi)$ and $\theta_e(\pi)$, and $R_e(\sigma)$ and $\theta_e(\sigma)$ are also shown.

C_6 (meV)	107 (±5)
C_5 (meV)	158 (±14)
C_4 (meV)	161 (±12)
C_3 (meV)	356 (±25)
C_2 (meV)	852 (±19)
C_1 (meV)	7 (±14)
$k^{(B)}$ (eV)	21.3
$K^{(A)}$ (eV)	12.5
$K^{(X)}$ (eV)	2.73
$D_e(\pi)$ (meV)	34 (±3)
$R_e(\pi)$ (Å)[a]	2.6 (±0.05)
$\theta_e(\pi)$ (°)[a]	90.0
$D_e(\sigma)$ (meV)	48 (±5)
$R_e(\sigma)$ (Å)[a]	5.3 (±0.1)
$\theta_e(\sigma)$ (°)[a]	0.0

[a]The definitions of R and θ are defined in text.

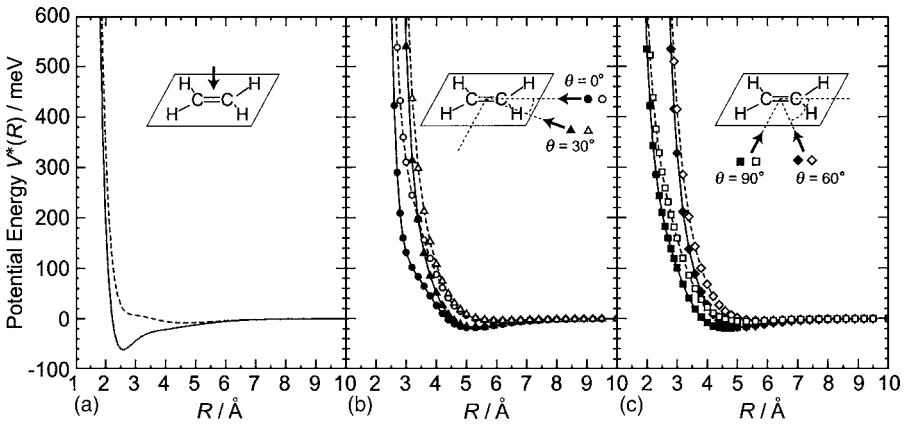

FIG. 9. (a) Optimized interaction potential energy curves (solid lines) of $V^*(R)$ and Li model potential curves (broken lines) $V_0(R)$ as a function of distance R between $He^*(Li)$ and the center of mass of C_2H_4 in the out-of-plane direction ($\theta=90°$ and $\phi=0°$). [(b) and (c)] $V^*(R)$ (solid lines+filled symbols) and $V_0(R)$ (broken lines +open symbols) in several in-plane configurations ($\phi=90°$) (circles: $\theta=0°$, triangles: $\theta=30°$, diamonds: $\theta=60°$, and squares: $\theta=90°$).

TABLE IV. Optimized parameters of the coefficients C_i in Eq. (6) for potential fitting and $K^{(i)}$ in Eq. (11) for ionization widths (see text) for the system of $C_2H_4+He^*(2\,^3S)$. The uncertainties of the coefficients C_i from the experimental errors of the observed slope parameters m are given in parentheses. The obtained potential well depths of $D_e(\pi)$ around the π_{CC} region, and their geometrical positions of $R_e(\pi)$, $\theta_e(\pi)$, and $\phi_e(\pi)$ are also shown.

C_7 (meV)	25 (±29)
C_6 (meV)	83 (±14)
C_5 (meV)	133 (±5)
C_4 (meV)	894 (±46)
C_3 (meV)	5 (±55)
C_2 (meV)	3859 (±39)
C_1 (meV)	3 (±63)
$K^{(C)}$ (eV)	19.8
$K^{(B)}$ (eV)	5.55
$K^{(A)}$ (eV)	6.17
$K^{(X)}$ (eV)	4.09
$D_e(\pi)$ (meV)	62 (±4)
$R_e(\pi)$ (Å)[a]	2.6 (±0.05)
$\theta_e(\pi)$ (°)[a]	90.0
$\phi_e(\pi)$ (°)[a]	0.0

[a]The definitions of R, θ, and ϕ are defined in text.

with the molecules through a charge donation to the vacant antibonding π^*_{CC} orbital.[62,63] In the equilibrium structures, the Li atom bridges the CC bond, which yields a triangle form by C–Li–C, and the CH bonds bend away from the Li atom. Thus, the structures of the hydrocarbon fragments in the complexes are rather different from those of the isolated hydrocarbons. From a computational investigation[64] by using the density functional theory, the binding energy (namely, attractive potential well) for the $Li+C_2H_2$ charge-transfer complex was estimated to be ca. 590 meV, and the Li atom was found to donate 0.72 electron to the π^*_{CC} orbital of the C_2H_2 fragment.

In the present system of $He^*+C_2H_2$ or C_2H_4, if collisional ionization occurs when the target molecule is deformed with the strong attractive interaction in the π_{CC} region as mentioned above, a large negative peak shift that nearly corresponds to the large attractive well depth and at least large band broadening to lower electron energies should be observed for the X ionic state in PIES.[10] However, such features have not been observed in the present measurements, and therefore a structural deformation of the hydrocarbon molecules that leads to a deep attractive well in the π_{CC} region is considered to be unlikely in the collisional ionization processes.

Relatively large negative values of the slope parameter m have also been observed in the higher E_c ranges (−0.18 for C_2H_2 in $200<E_c<320$ meV and −0.29 for C_2H_4 in $200<E_c<310$ meV), as shown in Tables I and II. However, judging from the magnitude of the optimized well depth [34 meV for $C_2H_2+He^*(2\,^3S)$ and 62 meV for $C_2H_4+He^*(2\,^3S)$], the negative CEDPICS in the higher E_c region is unlikely to arise from the attractive potential around the π_{CC} regions. In order to obtain further information on this, we have investigated the ionization probabilities as a function of the impact parameter b (opacity function). Figures 10 and 11 show the calculated opacity functions for $X\,^2\Pi_u$ ionic state of C_2H_2 and $X\,^2B_{2u}$ ionic state of C_2H_4, respectively. The interval for the lower collision energies of 20 and 30 meV is the same as that for the higher collision energies of 200 and 300 meV in the $\log\sigma$ (cross section) vs $\log E_c$ (collision energy) plots in Figs. 4 and 5.

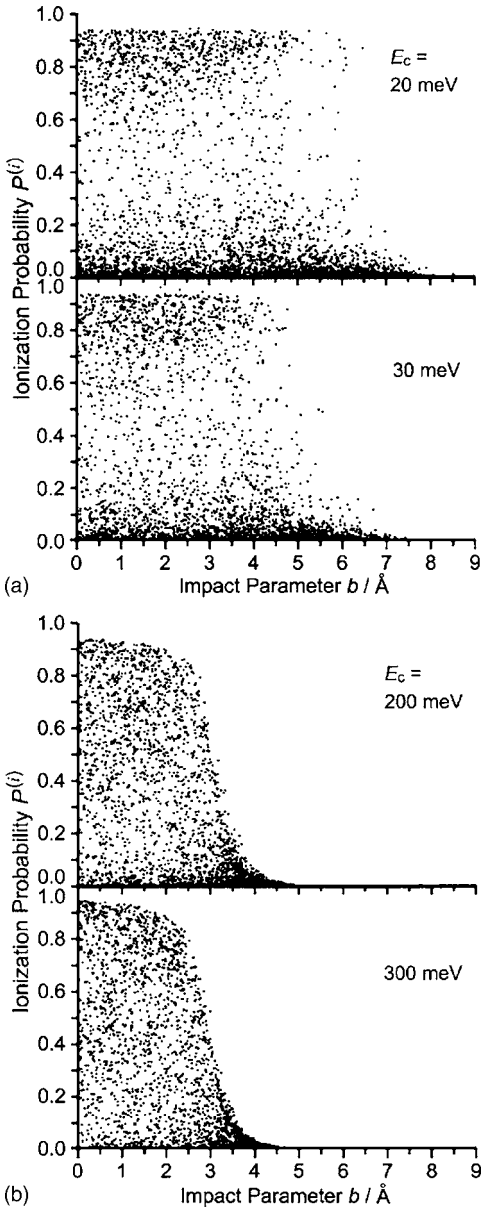

FIG. 10. Ionization probabilities as a function of the impact parameter b (opacity function) for producing $X\,^2\Pi_u$ ionic state of C_2H_2 in (a) the lower collision energies (20 and 30 meV) and (b) the higher collision energies (200 and 300 meV).

Since ionization probabilities depend not only on the impact parameter b but also on the molecular rotational motion and orientation, a large number of dots appear at a particular value of the impact parameter b; many different situations are involved in the same impact parameter. Since the sum of the partial ionization probabilities $P^{(i)}$ for each trajectory cannot exceed unity, one can see limited values of $P^{(i)}$ in the opacity functions. It can be recognized that impact collisions perpendicular to the CC axis of C_2H_2 and the molecular plane of C_2H_4 with zero impact parameter yield high ioniza-

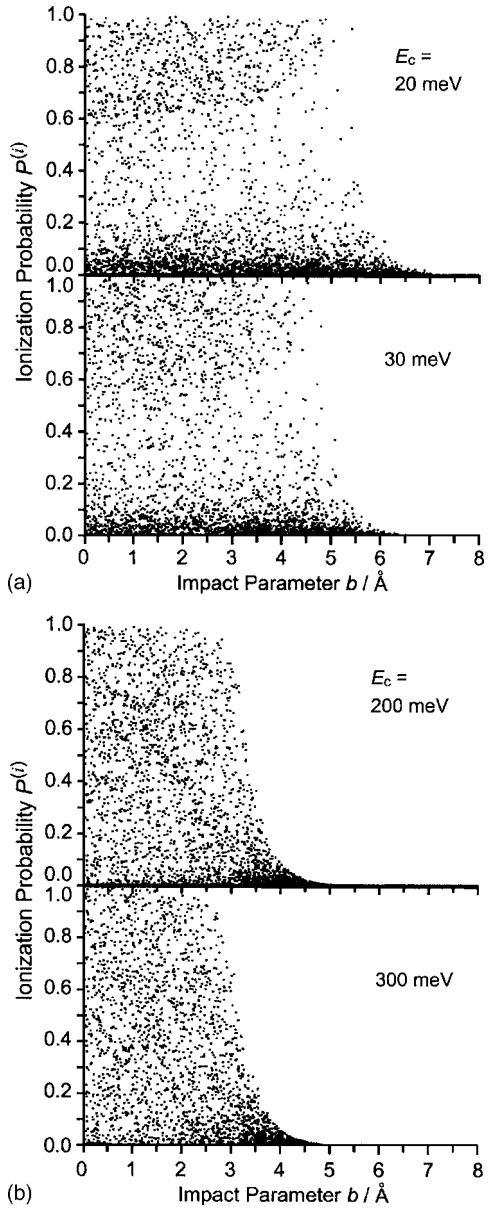

FIG. 11. Ionization probabilities as a function of the impact parameter b (opacity function) for producing $X\,^2B_{2u}$ ionic state of C_2H_4 in (a) the lower collision energies (20 and 30 meV) and (b) the higher collision energies (200 and 300 meV).

tion probabilities regardless of the collision energy, since the X ionic states for both molecules correspond to ionization from π_{CC} MOs that have a large electron density perpendicular to the CC axis or molecular plane.

As can be seen in Figs. 10(a) and 11(a) for the lower E_c range, the opacity functions largely depend on the collision energy. The critical impact parameters b_c rapidly decrease as the collision energy increases. As discussed in the previous theoretical studies on $CH_3CN+He^*(2\,^3S)$,[65] this feature clearly indicates that collisional ionization in the lower E_c region is governed by the attractive potential. On the other hand, in the higher collision energies of 200 and 300 meV [Figs. 10(b) and 11(b)], the critical impact parameters b_c (ca. 2.5–4.5 Å) are much smaller than those (ca. 5–7 Å) in the lower collision energies of 20 and 30 meV. This feature can support the above consideration that the attractive potential around the π_{CC} regions plays a minor role in collisional ionization into the X states in the higher collision energies. In addition, it is found that the hard-sphere collision regime as discussed above is not predominant in the higher collision energy range, since the maximum of the ionization probability at zero impact parameter is nearly the same in both collision energies of 200 and 300 meV. Accordingly, we may say that the observed negative slopes of CEDPICS in the higher E_c region are related to more or less a decrease in the effective time for metastable atoms to pass by the π_{CC} electron regions with the increase of collision energy, although the collisional ionization with small impact parameters (0–1 Å), which occurs in the repulsive potential around the π_{CC} region, also characterizes the CEDPICS in the higher E_c region.

D. Interaction potential in the σ electron region

Positive CEDPICS for ionization from σ orbitals in the higher collision energy region above ca. 100 meV is considered to be due to repulsive interaction around the σ_{CH} region (collinear direction) for C_2H_2 and the $\sigma_{CH(CC)}$ region (in-plane direction) for C_2H_4. In the case that "soft" repulsive interaction governs collisional ionization, ionization cross sections are expected to be larger with an increase of the collision energy, since a faster He^* atom compared to a slower He^* atom can reach more effectively the reactive region against the repulsive wall, which results in a large overlap between relevant orbitals.[23] As can be seen in the optimized PESs and potential energy curves [see Figs. 8(a), 9(b), and 9(c)], soft repulsive potential wall can be confirmed in the σ_{CH} region for C_2H_2 and the $\sigma_{CH(CC)}$ region for C_2H_4. Relative hardness of the repulsive potential wall around the H atom with respect to that around the middle position of the methylene (CH_2) unit was discussed in the previous study of the $C_2H_4+He^*(2\,^3S)$ system,[57] where a softer repulsive wall was suggested around the middle position of the CH_2 unit compared with the H atom. This can be confirmed by the optimized PES and potential energy curves $V^*(R)$ shown in Figs. 7(b) and 9(b).

On the other hand, in the lower collision energies between 20 and 50 meV, CEDPICS for ionization from σ orbitals shows a decreasing trend with an increase of the collision energy E_c (see the slope parameters m in Tables I and II). Furthermore, it has been found that the absolute value of the negative slope parameter m for C_2H_2 (the average value of m for two σ orbitals is −0.33) is much larger than that for C_2H_4 (the average value of m for three σ orbitals is −0.16). Based on the considerations on CEDPICS described in Sec. IV B, it is clear that the observed negative CEDPICS for ionization from σ orbitals in the lower E_c region can be related to attractive interaction in the σ_{CH} region for C_2H_2 and the $\sigma_{CH(CC)}$ region for C_2H_4. Thus, the observed curved structure with a minimum of the ionization cross section in CEDPICS (see Figs. 4 and 5) can be ascribed to transition from the attractive interaction regime ($E_c < D$) in the lower collision energies to the repulsive interaction regime ($E_c > D$) in the higher collision energies. In addition, from substantial difference of the observed slope parameters m in the

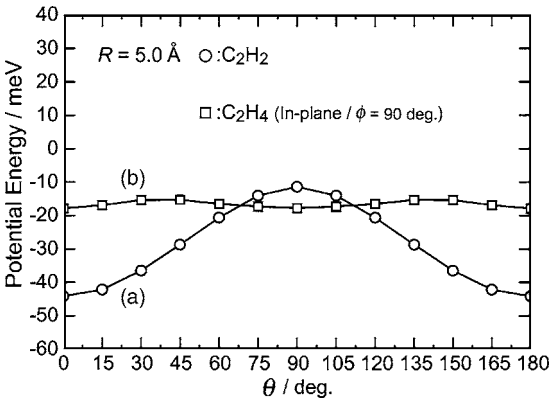

FIG. 12. The interaction potential energies as a function of the polar angle θ for (a) the $C_2H_2+He^*(2\,^3S)$ system (open circles) and (b) the $C_2H_4+He^*(2\,^3S)$ system [$\phi=90.0°$ (in plane), open squares] in the distance between the He^* atom and the center of mass of the target molecules $R=5.0$ Å.

lower E_c region, the attractive interaction in the σ_{CH} region for C_2H_2 is suggested to be much stronger than that for C_2H_4.

As can be seen in Figs. 6 and 8(a), an attractive potential well has been found around the H atom for the $C_2H_2+He^*(2\,^3S)$ system. The optimized well depth $D_e(\sigma)$ and its geometrical positions $R_e(\sigma)$ and $\theta_e(\sigma)$ were found to be 48 meV (ca. 1.1 kcal/mol), 5.3 Å, and 0.0°, respectively. On the other hand, in the case of C_2H_4, attractive potential surrounding the in-plane region has been found (Fig. 7). By averaging the potential minimum over the in-plane directions ($\phi=90°$, $\theta=0.0°$, 15.0°, 30.0°, 45.0°, 60.0°, 75.0°, and 90.0°), the mean value of the attractive well depths in the in-plane directions was found to be 18 meV (ca. 0.4 kcal/mol). Figure 12 compares the interaction potential energies between (a) the $C_2H_2+He^*(2\,^3S)$ system [open circles: θ=angle (variables)] and (b) the $C_2H_4+He^*(2\,^3S)$ system [open squares: $\phi=90.0°$ and θ=angle (variables)] in the distance between the He^* atom and the center of mass of the target molecules $R=5.0$ Å. In Fig. 12, it is obvious that a stereospecific attractive well is located around the H atom in the $C_2H_2+He^*(2\,^3S)$ system, while such a feature has not been found in the $C_2H_4+He^*(2\,^3S)$ system.

The optimized parameters of coefficients C_i for the Li model potential V_0 in Eq. (6) are also shown in Tables III and IV. The uncertainties of the coefficients C_i have been estimated simply by the experimental errors of the observed slope parameters m. By using the uncertainties of C_i, we have also evaluated the uncertainties of the optimized well depths D_e. Here, in order to show how the calculated CEDPICS is affected by the magnitude of the well depths D_e in PESs V^*, we have calculated CEDPICS when the values of the optimized well depths D_e listed in Table III and IV are varied by ±50%. Figure 13 compares the observed CEDPICS (open circles) for (a) $A\,^2\Sigma_g^+$ ionic state of $C_2H_2^+$ and (b) $X\,^2B_{2u}$ ionic state of $C_2H_4^+$ with the calculated CEDPICS by using the optimized PESs V^* (solid lines) and the trial PESs (dotted lines: +50% and broken lines: −50%) in the low collision energy range, where slopes of the observed CEDPICS are expected to be sensitive to the attractive potentials in

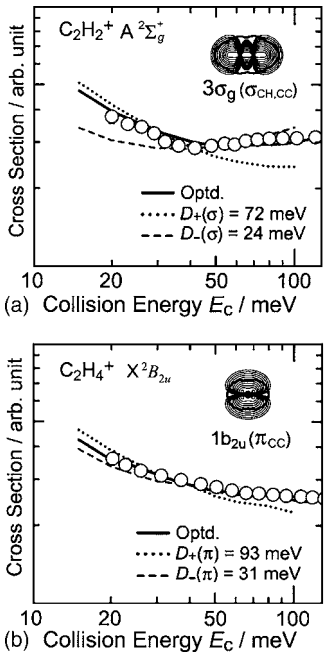

FIG. 13. Comparison of the observed CEDPICS (open circles) for (a) $A\,^2\Sigma_g^+$ ionic state of $C_2H_2^+$ and (b) $X\,^2B_{2u}$ ionic state of $C_2H_4^+$ with the calculated CEDPICS by using the optimized PESs V^* (solid lines) and trial PESs (see text). The CEDPICS obtained by the trial calculations is normalized with respect to the CEDPICS calculated by using the optimized PESs at $E_c=40$ meV.

PES. The CEDPICS obtained by the trial calculations is normalized with respect to the CEDPICS calculated by using the optimized PESs at $E_c=40$ meV, since here we focus on how the slopes of CEDPICS are varied by the trial calculations. It can be recognized from Fig. 13 that trial calculations fail to account for the observed slope of CEDPICS. In addition, it has been found that the observed CEDPICS in the lower E_c range is essential for evaluating weak attractive interaction as found in the present systems. Since the uncertainties of the optimized coefficients C_i are estimated by the experimental errors of the observed slope parameters in CEDPICS, it seems that considerably small values of the uncertainties of the well depths with ca. 10% are obtained.

In summary, it is clear that the global minimum in the PES of the $C_2H_2+He^*(2\,^3S)$ system is located around the H atom along the molecular axis (σ direction), while the π_{CC} electron region (π direction) shows dominant attractive potential in the $C_2H_4+He^*(2\,^3S)$ system. In Sec. IV F, such an attractive-site preference has been discussed in connection with the orbital interactions between the MOs of the unsaturated hydrocarbons and the atomic orbitals of the metastable atom.

E. General remarks on the potential corrections

Here, the roles of the C_i parameters in the corrections for the Li model potential V_0 in Eq. (6) are discussed based on the principles of orbital interactions. As can be seen in Tables III and IV, the optimized coefficients of C_i in Eq. (6) are all positive. This indicates that the potential energy surfaces V^* for $He^*(2\,^3S)$ are pulled down to the lower energies from the Li model potential V_0. From the difference of the IP between

Li(2 ^2S) (5.392 eV) and He*(2 ^3S) (4.768 eV), the energy level of the 2*s* electron of He*(2 ^3S) can be considered to be much higher in comparison with that of Li(2 ^2S). Taking the energy gaps between the 2*s* electron between the MOs of the target molecules into account, contributions to energy lowering in the Li model potentials V_0 are expected to be overestimated for the occupied MOs and underestimated for the unoccupied MOs. This argument leads to negative coefficients C_i for the occupied MOs and positive coefficients C_i for the unoccupied MOs in Eq. (6). For the occupied MOs, however, the optimized coefficients C_1-C_3 for C_2H_2 and C_1-C_4 for C_2H_4 show positive values (see Tables III and IV) contrary to the above expectation.

It should be of note that in the interacting system of He*(Li)+C_2H_2 or C_2H_4 (closed-shell molecules), the 2*s* unpaired electron in the singly occupied orbital has an antibonding character. In connection with this, the contributions of vacant 2*p* orbitals leading to 2*s*-2*p* hybridization of He*(Li) atom should be considered;[26,29,66,67] when the contribution of 2*s*-2*p* hybridization increases, electron overlap repulsion with the target molecules decreases due to the small lobe of the 2*s*-2*p* hybridization. Therefore, this effect contributes also to the energy lowering in the Li model potentials V_0. Since the energy gap between the 2*s* and 2*p* orbitals of He*(2 ^3S) (1.114 eV) is much smaller than that of Li(2 ^2S) (1.848 eV), the hybridization effect is underestimated in the Li model potential V_0 in Eq. (6). As discussed previously,[42] since the 2*s*-2*p* orbital mixing is caused via interactions with the occupied MOs, positive coefficients C_i for the occupied MOs can be expected, if the hybridization effect lowering the unpaired electron level in the interacting system is much more important than the energy-lowering effects on the paired electron levels for occupied orbitals. Thus, the positive coefficients for the occupied MOs listed in Tables III and IV suggest that the 2*s*-2*p* hybridization effect predominantly contributes to corrections of the Li model potentials V_0. Concerning the above discussion, we have to mention a propensity that potential energy curves for Li+*X* (*X*=H, Li, Na, K, Ca, and Hg) are more attractive than those for He*+*X*,[41] which is contrary with the present studies for molecular targets. For open-shell atomic targets, however, it can be recognized from the above discussion based on orbital interactions between He*(Li) and targets, the 2*s* electron of He*(Li) occupies an orbital having a bonding character in the interacting system. In this case, the 2*s*-2*p* hybridization effect has a minor contribution for attractive well in the potential energy curves, while the orbital interaction between the 2*s* electron of He*(Li) and the unpaired *ns* electron of atomic targets plays a dominant role for the attractive well. Although atomic targets investigated in the previous work[41] also involve closed-shell atoms, this can be connected to the different trends in the potential energy curves for the atomic targets with respect to the PESs for the molecular targets.

F. The preference for attractive site in unsaturated hydrocarbons

In the overlap correction method employed in the present study, it has been found that the positive coefficients C_i of the unoccupied MOs have a dominant contribution in lowering the potential energy of V_0 in Eq. (6) at long ranges.[42] As discussed previously,[42,44] the positive contribution of C_i for the unoccupied MOs supplements a charge-transfer (CT) interaction effect leading to $M^{\delta-}A^{*\delta+}$ (Refs. 68–70) in the correction of Li model potential V_0. As discussed in Sec. IV D, the energy level of the 2*s* electron of He*(2 ^3S) is much higher in comparison with that of Li(2 ^2S), and the energy gaps between the 2*s* atomic orbital and unoccupied MOs of a target molecule become much smaller for He*(2 ^3S). From this point of view, it follows that the CT interaction, namely, the orbital interaction between the 2*s* atomic orbital and unoccupied MOs of a target molecule, is much more important in the case of He*(2 ^3S).

In the previous study on the CH_3CN+He*(2 ^3S) system, a stereospecific attractive well with a depth of ca. 40 meV around the methyl group ($-CH_3$) has been found.[44] The attractive well is located in the C-atom side along the CCN axis at a distance of 5.80 Å from the center of mass of CH_3CN. From the analysis of the optimized coefficients it has been concluded that the attractive potential around the methyl group ($-CH_3$) can be related to the orbital interaction between the 2*s* atomic orbital of He*(2 ^3S) metastable atom and the σ-type unoccupied MO ($8a_1$) of CH_3CN that has a large extent of the electron distribution around the methyl group.[44] It is worth noting that a similar feature around the methyl group has been obtained by semiempirical calculations for the anisotropic interaction potential for the CH_3Cl +Ne* system,[70,71] where the attractive potential well in the methyl group has been ascribed to the CT interaction effect, since the lowest unoccupied molecular orbital (LUMO) of CH_3Cl has a σ^* C–Cl character.[71]

As listed in Table III, the coefficients C_i of the low-lying unoccupied MOs with σ symmetry ($4\sigma_g$ and $3\sigma_u$) show a relatively large positive value in the case of C_2H_2. It should be noted that both the unoccupied σ-type MOs of $4\sigma_g$ and $3\sigma_u$ have a large extent of the electron distribution in the collinear direction to the molecular axis (HCCH), as can be seen in Fig. 1(a). Therefore, it is obvious that the stereospecific attractive well on the H atom of C_2H_2 found in the present study can be ascribed to the orbital interactions between the 2*s* atomic orbital of He*(2 ^3S) and the σ-type unoccupied MOs ($4\sigma_g$ and $3\sigma_u$) that leads to the CT interaction effect, although the 2*s*-2*p* hybridization effect is considered to cause the attractive well at the partially negatively charged site in the target molecules.[26]

In the case of the C_2H_4+He*(2 ^3S) system, the coefficients C_i of the low-lying unoccupied MOs having σ^* character ($4a_g$ and $3b_{1u}$) also show relatively large positive values. However, the spatial distribution of electron density for the $4a_g$ and $3b_{1u}$ unoccupied MOs is clearly different from each other, as can be seen in Fig. 1(b). Therefore, in the case of the C_2H_4+He*(2 ^3S) system it can be understood that the contributions of the $4a_g$ and $3b_{1u}$ unoccupied MOs yield an attractive potential surrounding the in-plane region. The observed nearly the same slope parameters *m* for the σ-type MOs [$m=-0.17$ for $1b_{2g}(\sigma_{CH})$, -0.18 for $3a_g(\sigma_{CC})$, and -0.13 for $1b_{3u}(\sigma_{CH})$] in the lower E_c region (20–50 meV) can account for the shallow attractive potential in the in-

plane directions. The substantial difference in the observed negative slope parameters m between C_2H_2 and C_2H_4 in the lower E_c region (the averaged value of m for two σ orbitals in C_2H_2 is −0.33, while that of m for three σ orbitals is −0.16) can also be explained by the optimized PESs as shown in Figs. 6–9, where the stereospecific attractive potential on the H atom of C_2H_2 is clearly related to much larger negative values of m in the lower E_c region for C_2H_2.

It is interesting that one can find a correlation between the orbital energies of the low-lying unoccupied MOs and their optimized coefficients C_i in the potential corrections. The orbital energies of $4\sigma_g$ and $3\sigma_u$ for C_2H_2 obtained by the SCF-MO calculation with a 6-311++G^{**} basis set are 1.15 and 1.29 eV, respectively. On the other hand, the energy values of $4a_g$ and $3b_{1u}$ for C_2H_4 obtained by the same method and basis set are 1.33 and 1.68 eV, respectively. From these results, it is clear that the orbital interactions between the $2s$ atomic orbital of a $He^*(2\,^3S)$ metastable atom and unoccupied σ-type MOs are much more important for the C_2H_2 $+He^*(2\,^3S)$ system, because of its smaller energy gaps between the relevant orbitals. This can be confirmed by the optimized coefficients C_i listed in Tables III and IV, where the coefficients C_4 and C_5 (corresponding to $4\sigma_g$ and $3\sigma_u$ MOs, respectively) for C_2H_2 show much larger values than the coefficients C_5 and C_6 (corresponding to $4a_g$ and $3b_{1u}$ MOs, respectively) for C_2H_4. In connection with this, electron affinities (EAs) for the unsaturated hydrocarbons should be referred here. The experimental values of the vertical EAs for C_2H_2 and C_2H_4 were reported to be −2.6 and −1.78 eV, respectively, in electron transmission spectroscopy with low energy electrons.[72,73] These values were obtained from a shape resonance to $^2\Pi_g$ state of the respective anions observed in the total electron scattering cross sections as a function of incident electron energy. Since these temporary anion states are associated with low-lying π^* orbitals of the unsaturated hydrocarbons that contribute the sharp structures of the shape resonance on the observed electron transmission spectra, the above EAs for the unsaturated hydrocarbons cannot be compared with the present calculated results.

Finally, we shall discuss the attractive potential well at the π_{CC} electron region in the unsaturated hydrocarbons. From the previous studies on the molecules with π_{CC} electrons,[25,42,57,74] the attractive interaction in the π electron region is likely to be related to the orbital interactions between the $2s$ and vacant $2p$ atomic orbitals of $He^*(2\,^3S)$ and the high-lying occupied π orbitals. The highest occupied molecular orbitals (HOMOs) of the present unsaturated hydrocarbons are $1\pi_u(\pi_{CC})$ for C_2H_2 and $1b_{2u}(\pi_{CC})$ for C_2H_4. It should be noted here that the IPs for the HOMOs have been reported to be 11.40 eV for C_2H_2 and 10.51 eV for C_2H_4.[55] This indicates that the energy level of HOMO for C_2H_4 is much higher than that for C_2H_2. Therefore, it follows that the orbital interactions between the relevant orbitals are much more significant for C_2H_4, which can be related to the attractive-site preference of the π direction in the C_2H_4 $+He^*(2\,^3S)$ system. It is also interesting to note that this is in contrast with the case of the unoccupied MOs as mentioned above.

V. CONCLUSION

The state-resolved collision energy dependence of the Penning ionization cross sections for the unsaturated hydrocarbons (C_2H_2 and C_2H_4) with $He^*(2\,^3S)$ metastable atoms was observed in a wide collision energy range from 20 to 350 meV. A recently developed cooled discharge nozzle source for producing low velocity $He^*(2\,^3S)$ metastable beams has enabled us to survey weak attractive interaction for the present systems as well as to evaluate the PESs. Based on the comparison of the observed CEDPICS with the classical trajectory calculations, PESs for the interacting systems were obtained from optimizations of *ab initio* Li model potentials utilizing the overlap correction method. It is found that in the $C_2H_2+He^*(2\,^3S)$ system, the global minimum with a well depth of 48 meV (ca. 1.1 kcal/mol) is located around the H atom along the molecular axis. On the other hand, in the $C_2H_4+He^*(2\,^3S)$ system, a dominant attractive well has been found in the π_{CC} electron region [the well depth is 62 meV (ca. 1.4 kcal/mol)].

From the optimized potential parameters of the target MOs and analysis of the orbital energies, it is concluded that the orbital interactions between σ-type unoccupied MOs of $4\sigma_g$ and $3\sigma_u$ in C_2H_2 and the $2s$ atomic orbital of $He^*(2\,^3S)$ can account for the stereospecific attractive well around the H atom (σ direction), while HOMO of C_2H_4 with a π_{CC} character plays a significant role for the preference of the attractive site in the π_{CC} electron region (π direction).

ACKNOWLEDGMENTS

The present work was supported by a Grant in Aid for Scientific Research from the Ministry of Education, Culture, Sports, Science, and Technology (MEXT). Two of the authors (T.H. and S.M.) are supported by the Research Fellowship of the Japan Society for the Promotion of Science for Young Scientists.

[1] H. Loesch, J. Phys. Chem. **101**, 7461 (1997), special issue on stereodynamics.
[2] D. J. Nesbitt, Chem. Rev. (Washington, D.C.) **88**, 843 (1988).
[3] R. E. Miller, Science **240**, 447 (1988).
[4] L. Beneventi, P. Casavecchia, F. Vecchiocattivi, G. G. Volpi, U. Buck, C. Lauenstein, and R. Schinke, J. Chem. Phys. **89**, 4671 (1989).
[5] U. Buck, I. Ettischer, S. Schlemmer, M. Yang, P. Vohralik, and R. O. Watts, J. Chem. Phys. **99**, 3494 (1993).
[6] M. Yang and R. O. Watts, J. Chem. Phys. **100**, 3582 (1994).
[7] D. Cappelletti, M. Bartolomei, F. Pirani, and V. Aquilanti, J. Phys. Chem. A **106**, 10764 (2002).
[8] V. Aquilanti, M. Bartolomei, F. Pirani, D. Cappelletti, F. Vecchiocattivi, Y. Shimizu, and T. Kasai, Phys. Chem. Chem. Phys. **7**, 291 (2005).
[9] F. M. Penning, Naturwiss. **15**, 818 (1927).
[10] A. Niehaus, Adv. Chem. Phys. **45**, 399 (1981).
[11] S. Y. Tang, A. B. Marcus, and E. E. Muschlitz, Jr., J. Chem. Phys. **56**, 566 (1972).
[12] E. Illenberger and A. Niehaus, Z. Phys. B **20**, 33 (1975).
[13] A. Pesnelle, G. Watel, and C. Manus, J. Chem. Phys. **62**, 3590 (1975).
[14] T. P. Parr, D. M. Parr, and R. M. Martin, J. Chem. Phys. **76**, 316 (1982).
[15] L. Appolloni, B. Brunetti, J. Hermanussen, F. Vecchiocattivi, and G. G. Volpi, J. Chem. Phys. **87**, 3804 (1987).

[16] R. Feltgen, H. Ferkel, R. K. B. Helbing, A. Lindinger, D. Pikorz, and H. Vehmeyer, J. Chem. Phys. **111**, 7298 (1999).
[17] H. Hotop and A. Niehaus, Z. Phys. **228**, 68 (1969).
[18] V. Čermák, J. Chem. Phys. **44**, 3781 (1966).
[19] A. J. Yencha, in *Electron Spectroscopy: Theory, Techniques and Applications*, edited by C. R. Brundle and A. D. Baker (Academic, New York, 1984), Vol. 5.
[20] K. Ohno, H. Mutoh, and Y. Harada, J. Am. Chem. Soc. **105**, 4555 (1983).
[21] K. Ohno, S. Matsumoto, and Y. Harada, J. Chem. Phys. **81**, 4447 (1984).
[22] K. Mitsuke, T. Takami, and K. Ohno, J. Chem. Phys. **91**, 1618 (1989).
[23] K. Ohno, T. Takami, K. Mitsuke, and T. Ishida, J. Chem. Phys. **94**, 2675 (1991).
[24] D. C. Dunlavy, D. W. Martin, and P. E. Siska, J. Chem. Phys. **93**, 5347 (1990).
[25] T. Takami and K. Ohno, J. Chem. Phys. **96**, 6523 (1992).
[26] P. E. Siska, Rev. Mod. Phys. **65**, 337 (1993).
[27] F. Biondini, B. G. Brunetti, P. Candori, F. De Angelis, S. Falcinelli, F. Tarantelli, M. M. Teixidor, F. Pirani, and F. Vecchiocattivi, J. Chem. Phys. **122**, 164307 (2005).
[28] K. Ohno, H. Yamakado, T. Ogawa, and Y. Yamata, J. Chem. Phys. **105**, 7536 (1996).
[29] J. S. Cohen and N. F. Lane, J. Chem. Phys. **66**, 586 (1977).
[30] A. P. Hickman, A. D. Isaacson, and W. H. Miller, J. Chem. Phys. **66**, 1492 (1977).
[31] T. Ishida, Chem. Phys. Lett. **191**, 1 (1992).
[32] T. Ishida and K. Horime, J. Chem. Phys. **105**, 5380 (1996).
[33] H. Nakamura, J. Phys. Soc. Jpn. **26**, 1473 (1969).
[34] W. H. Miller, J. Chem. Phys. **52**, 3563 (1970).
[35] F. A. U. Thiel, L. Thiel, A. J. Yencha, M.-W. Ruf, W. Meyer, and H. Hotop, J. Phys. B **37**, 3691 (2004).
[36] L. Thiel, H. Hotop, and W. Meyer, J. Chem. Phys. **122**, 184309 (2005).
[37] T. Ogawa and K. Ohno, J. Chem. Phys. **110**, 3773 (1999).
[38] E. W. Rothe, R. H. Neynaber, and S. Trujillo, J. Chem. Phys. **42**, 3310 (1965).
[39] H. Hotop, Radiat. Res. **59**, 379 (1974).
[40] H. Haberland, Y. T. Lee, and P. E. Siska, Adv. Chem. Phys. **45**, 487 (1981).
[41] H. Hotop, T. E. Roth, M.-W. Ruf, and A. J. Yencha, Theor. Chem. Acc. **100**, 36 (1998).
[42] S. Maeda, M. Yamazaki, N. Kishimoto, and K. Ohno, J. Chem. Phys. **120**, 781 (2004).
[43] K. Ohno, M. Yamazaki, S. Maeda, and N. Kishimoto, J. Electron Spectrosc. Relat. Phenom. **142**, 283 (2005).
[44] T. Horio, M. Yamazaki, S. Maeda, T. Hatamoto, N. Kishimoto, and K. Ohno, J. Chem. Phys. **123**, 194308 (2005).
[45] M. Yamazaki, S. Maeda, N. Kishimoto, and K. Ohno, J. Chem. Phys. **122**, 044303 (2005).
[46] T. Horio, T. Hatamoto, N. Kishimoto, and K. Ohno, Chem. Phys. Lett. **397**, 242 (2004).
[47] T. Hsu and J. L. Hirshfield, Rev. Sci. Instrum. **47**, 236 (1976).
[48] G. Beamson, H. Q. Porter, and D. W. Turner, J. Phys. E **13**, 64 (1980).
[49] G. Beamson, H. Q. Porter, and D. W. Turner, Nature (London) **290**, 556 (1981).
[50] Y. Yamakita, H. Tanaka, R. Maruyama, H. Yamakado, F. Misaizu, and K. Ohno, Rev. Sci. Instrum. **71**, 3042 (2000).
[51] M. J. Frisch, G. W. Trucks, H. B. Schlegel *et al.*, GAUSSIAN 94, Revision C.3, Gaussian, Inc., Pittsburgh, PA, 1995.
[52] S. F. Boys and F. Bernardi, Mol. Phys. **19**, 553 (1970).
[53] W. H. Miller and H. Morgner, J. Chem. Phys. **67**, 4923 (1977).
[54] R. S. Mulliken, J. Chim. Phys. Phys.-Chim. Biol. **46**, 497 (1949).
[55] K. Kimura, S. Katsumata, Y. Achiba, T. Yamazaki, and S. Iwata, *Handbook of He I Photoelectron Spectra of Fundamental Organic Molecules* (Japan Scientific, Tokyo, 1981).
[56] T. Takami, K. Mitsuke, and K. Ohno, J. Chem. Phys. **95**, 918 (1991).
[57] K. Ohno, K. Okamura, H. Yamakado, S. Hoshino, T. Takami, and M. Yamauchi, J. Phys. Chem. **99**, 14247 (1995).
[58] T. Ueno and Y. Hatano, Oyo Butsuri **47**, 1006 (1978).
[59] K. L. Bell, A. Dalgarno, and A. E. Kingston, J. Phys. B **1**, 18 (1968).
[60] N. C. Handy, M. T. Marron, and H. J. Silverstone, Phys. Rev. **180**, 45 (1969).
[61] M. M. Morrell, R. G. Parr, and M. Levy, J. Chem. Phys. **62**, 549 (1975).
[62] P. H. Kasai, J. Am. Chem. Soc. **114**, 3299 (1992).
[63] L. Manceron, A. Schrimpf, T. Bornemann, R. Rosendahl, F. Faller, and H.-J. Stöckmann, Chem. Phys. **169**, 219 (1993).
[64] L. A. Eriksson, J. Wang, and R. J. Boyd, Chem. Phys. Lett. **235**, 422 (1995).
[65] T. Ogawa and K. Ohno, J. Phys. Chem. A **103**, 9925 (1999).
[66] A. D. Isaacson, A. P. Hickman, and W. H. Miller, J. Chem. Phys. **67**, 370 (1977).
[67] P. E. Siska, J. Chem. Phys. **71**, 3942 (1979).
[68] J. L. Magee, J. Chem. Phys. **8**, 687 (1940).
[69] V. Aquilanti, D. Cappelletti, and F. Pirani, Chem. Phys. Lett. **271**, 216 (1997).
[70] B. Brunetti, P. Candori, J. De Andres, F. Pirani, M. Rosi, S. Falcinelli, and F. Vecchiocattivi, J. Phys. Chem. A **101**, 7505 (1997).
[71] M. Albertí, J. M. Lucas, B. Brunetti, F. Pirani, M. Stramaccia, M. Rosi, and F. Vecchiocattivi, J. Phys. Chem. A **104**, 1405 (2000).
[72] P. D. Burrow and K. D. Jordan, Chem. Phys. Lett. **36**, 594 (1975).
[73] K. D. Jordan and P. D. Burrow, Acc. Chem. Res. **11**, 341 (1978).
[74] H. Yamakado, K. Okamura, K. Ohshimo, N. Kishimoto, and K. Ohno, Chem. Lett. **1997**, 269.